

Copper(II) Pyridyl Aminophenolates: Hypoxia-Selective, Nucleus-Targeting Cytotoxins, and Magnetic Resonance Probes

Kathleen E. Prosser, [a, b] Da Xie, [b] Annica Chu, [a] Gregory A. MacNeil, [a] Bryton R. Varju, [a] Rahul T. Kadakia, [b] Emily L. Que, *[b] and Charles J. Walsby*[a]

Abstract: Targeting the low-oxygen (hypoxic) environments found in many tumours by using redox-active metal complexes is a strategy that can enhance efficacy and reduce the side effects of chemotherapies. We have developed a series of Cu^{II} complexes with tridentate pyridine aminophenolate-based ligands for preferential activation in the reduction window provided by hypoxic tissues. Furthermore, ligand functionalization with a pendant CF₃ group provides a ¹⁹F spectroscopic handle for magnetic-resonance studies of redox processes at the metal centre and behaviour in cellular environments. The phenol group in the ligand backbone was substituted at the *para* position with H, Cl, and NO₂ to modulate the reduction potential of the Cu^{II} centre, giving a range of values below the window expected for hypoxic

tissues. The NO₂-substituted complex, which has the highest reduction potential, showed enhanced cytotoxic selectivity towards HeLa cells grown under hypoxic conditions. Cell death occurs by apoptosis, as determined by analysis of the cell morphology. A combination of ¹⁹F NMR and ICP-OES indicates localization of the NO₂ complex in HeLa cell nuclei and increased cellular accumulation under hypoxia. This correlates with DNA nuclease activity being the likely origin of cytotoxic activity, as demonstrated by cleavage of DNA plasmids in the presence of the Cu^{II} nitro complex and a reducing agent. Selective detection of the paramagnetic Cu^{II} complexes and their diamagnetic ligands by ¹⁹F MRI suggests hypoxia-targeting theranostic applications by redox activation.

Introduction

Dose-limiting toxicity is a hurdle confronting the clinical application of many chemotherapeutics. This typically arises from insufficient discrimination in cytotoxicity between cancerous and normal cells. A compelling example of this is cisplatin, a platinum(II)-based therapeutic employed in many chemotherapeutic regimes, which exhibits a variety of severe side effects. This off-target activity arises from the primary mechanism of action of cisplatin involving binding to DNA. Although this process leads to apoptosis, there is little selectivity between the DNA of cancerous and healthy tissues. [2]

Several different strategies have been developed to endow anticancer compounds with selectivity, such as the inclusion of targeting groups that interact with specific cancer associated biomolecules.^[3] A promising approach is to capitalize on the

differences between the microenvironments of tumours and healthy tissues. One such difference is lower oxygen concentrations (hypoxia) that arise from accelerated growth and lack of vasculature in tumours associated with certain cancers.^[4]

These reduced oxygen levels result in a lower overall biological reduction potential, and can also lead to greater acidity and altered cellular growth.^[5] Furthermore, hypoxic tumours can be resistant to traditional treatments, including radiation therapy and many chemotherapies.^[6] As hypoxia is not typically observed in healthy tissues, several organic and metal-based redox-active therapies have been developed to selectively exploit the difference in environments.^[7] In the case of platinum chemotherapeutic candidates, Pt^{IV} prodrugs have been employed, which upon reduction in hypoxic environments selectivley produce cytotoxic Pt^{III} species.^[8]

Research into copper anticancer compounds is one of the most active areas currently in medicinal inorganic chemistry and a wide array of copper complexes have been studied for their chemotherapeutic potential. Prominent examples include complexes of: i) thiosemicarbazone, ii) Schiff base, iii) imidazole, benzimidazole, triazole, and iv) bipyridine and phenanthroline ligands. The anticancer activity of copper complexes frequently has been linked to increased oxidative stress, with Cu^{II} complexes promoting generation of reactive oxygen species (ROS) or depletion of glutathione (GSH). Other mechanisms include DNA binding, proteasome inhibition, and inhibition of topoisomerases. Reduction of Cu^{II} complexes under biological conditions can initiate redox

 [[]a] Dr. K. E. Prosser, A. Chu, G. A. MacNeil, B. R. Varju, Prof. C. J. Walsby Department of Chemistry,
 Simon Fraser University
 8888 University Dr., Burnaby, BC V5A 1S6 (Canada)
 E-mail: cwalsby@sfu.ca

[[]b] Dr. K. E. Prosser, Dr. D. Xie, R. T. Kadakia, Prof. E. L. Que Department of Chemistry The University of Texas at Austin 105 E. 24th Street Stop A5300, Austin, TX 78712 (USA) E-mail: emilyque@cm.utexas.edu

Supporting information for this article is available on the WWW under https://doi.org/10.1002/chem.202100603



cycling to produce toxic ROS, through Fenton-like chemistry, which can then damage biomolecules and cellular components.^[14] This potentially enables targeting of the reduction window in hypoxic tumour tissues for selective activation. Copper complexes are particularly suitable for this strategy since the Cu^{II}/Cu^{II} couple can be tuned over a wide range of potentials through ligand design. Consequently, ROS generation can be limited to tumour tissues in vivo.^[96,17]

Cu^{II} complexes have also shown promise as imaging agents for tracking redox processes in biological environments. The ability to characterize the in vivo spatial distribution of Cu^{II} (d⁹, $S=^1/_2$), Cu^{II} (d¹⁰, S=0) and released ligands can provide information on the anticancer mechanisms of these compounds and the reducing environments of tumour tissues. Changes in the coordination sphere of paramagnetic Cu^{II} centres in biologically-relevant conditions are traditionally evaluated by electron paramagnetic resonance (EPR) methods. However, EPR can only provide information on reduction processes affecting Cu^{II} centres by detecting loss of signal, and in vivo EPR imaging is limited to radical species. Equation 120.

Alternatively, NMR and nuclear magnetic resonance-based imaging methods are showing promise for characterizing the effects of hypoxia and the behaviour of metal-based therapeutic candidates in vivo.[21] The proof-of-principle application of these approaches has been demonstrated using copper thiosemicarbazonate complexes such as diacetylbis(N(4)-methylthiosemicarbazonato) copper(II); CuATSM (Figure S1 in the Supporting Information). [17b,18a,b,22] In these compounds, and the complexes in this report (Figure 1a), functionalization with a fluorinated tag enables NMR and imaging studies. Magnetic resonance (MR) characterization of the spatial distribution of these, and other fluorinated molecules is commonly referred to as magnetic resonance imaging (MRI),[18a,23] and this terminology is used here. However, in some fields, such measurements are classified as magnetic resonance spectroscopy (MRS), with "MRI" reserved for the proton resonance of water. [24]

¹⁹F is potentially an excellent nucleus for the development of diagnostic agents due to the suitable NMR properties of ¹⁹F nuclei ($I=\frac{1}{2}$, 100% abundance, receptivity vs. $^{1}H=0.8328$), and the negligible concentration of fluorine in the human body. [25] As a complimentary technique to traditional ¹H MRI, ¹⁹F MRI employing paramagnetic agents has been implemented to pН, ROS in probe hypoxia, and biological environments.[18a,b,d,e,21b,23b,26] Fluorine-decorated molecules have also been used as theranostic (therapeutic + diagnostic) chemotherapeutic imaging agents, allowing for the study of the distribution, metabolism, and mechanisms of these compounds by MR methods.[27]

Herein, we demonstrate the potential of ¹⁹F-tagged metal complexes to function both as hypoxia-selective cytotoxic agents and ¹⁹F magnetic resonance probes. The reduction potentials of the Cu^{II}-based pyridine aminophenolate complexes used in these studies (Figure 1) were tuned by *para* substitution of the ligand phenol. This enabled targeting of the hypoxic reduction window. A trifluoromethyl (CF₃) group attached to the ligand scaffold enabled the study of these complexes through ¹⁹F NMR and MRI methods, providing

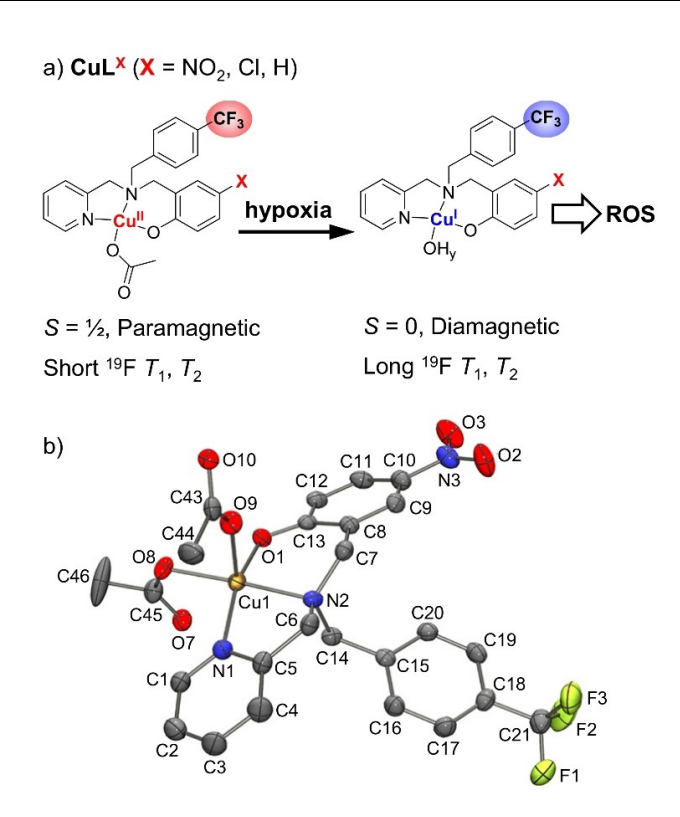


Figure 1. a) Fluorinated Cu^{II} complexes CuL^{X} and the turn-on of their cytotoxic and MR imaging properties in hypoxic environments. Number of protons, y, equals 1 or 2. b) X-ray crystal structure of CuL^{NO_2} with ellipsoids at the 50% probability level.

insight into their mechanism of action. This combination of therapeutic and diagnostic properties is a step towards theranostic molecules that have the potential to both identify and selectively activate in hypoxic tumour tissues.

Results and Discussion

Synthesis and characterization

Cu^{II} complexes CuL^X (X=NO₂, Cl, H) were prepared in three steps starting with reaction of 2-picolylamine with the appropriate salicylaldehyde to generate the imine in situ, followed by reduction to the corresponding amine PAPX (Scheme S1). The amine was alkylated to produce fluorinated ligands CF₃PAPX in moderate yields (36–73%). Metallation was carried out in MeOH with Cu(OAc)₂ with triethylamine as a base, giving the CuL^X complexes in good yields (83–89%) following recrystallization in acetone.

Crystals of CuL^{NO2} suitable for x-ray crystallography (Figure 1) were obtained from a concentrated solution in MeOH. CuL^{NO2} crystallizes in the chiral Pca2₁ space group, and the crystal structure consists of polymeric 1D chains made up of two crystallographically distinct CuL^{NO2} units that are bridged through acetate ligands (Figure S4). The Cu^{II} centres have a square pyramidal coordination geometry incorporating tridentate coordination from the CF₃PAPNO₂ ligand and two mono-



dentate acetate ligands; the equatorial and axial Cu-O acetate bonds have lengths of 1.965 and 2.221 Å respectively (see Tables S2 and S3 for bond lengths and angles). The polymeric structure is likely a consequence of crystal packing, with the axial acetate dissociating in solution to give mononuclear Cu $^{\parallel}$ species. This was confirmed by frozen-solution EPR spectra of the CuL $^{\times}$ complexes, which are characteristic of mononuclear S=1/2 Cu $^{\parallel}$ species (Figure S28), with no indication of exchange coupling between Cu centres. The average Cu-F distance is 9.1 Å, which is close enough to observe paramagnetic relaxation enhancement effects^[28] of the Cu $^{\parallel}$ centre in 19 F NMR spectra. $^{[29]}$

Solution behaviour

Ligand-exchange reactions are important mechanistic features of many metal-based therapeutics, with aquation or binding to biomolecules often resulting in prodrug activity. [7a,30] This is particularly significant for Cu^{II} complexes since they are typically labile and can exchange ligands under physiological conditions. [12b,31] To characterize changes in the ligand environment of CuL^X following aqueous dissolution, 50 μ M solutions of each complex in MES buffer (pH 6.5), were monitored by UV/Vis spectroscopy over 12 hours at 37 °C. Under these conditions, no changes in their absorption spectra were observed. However, ¹H NMR spectra of the complexes in D₂O show a signal from free acetate at 2.28 ppm (Figure S20). Thus, it can be concluded that the complexes initially undergo rapid loss of acetate to give aquo or hydroxo species but no subsequent ligand exchange occurs.

UV/Vis spectra of CuL^X were measured in DMSO at higher concentrations to evaluate d-d transitions (Figure S25); these measurements were not possible in aqueous solutions because of limited solubility. The λ_{max} of the d-d transitions shifted to lower wavelength across the series: CuL^{NO2} > CuL^{CI} > CuL^H; corresponding to increasing d-orbital splitting (Table 1). This trend shows that *para* substitution of the phenol functionality of the CF₃PAPX ligands has the desired effect of modulating the electronic properties of the Cu^{II} centre.

The coordination spheres of the CuL^X complexes in aqueous buffer were also characterized by EPR. Measurements of 500 μ M CuL^X frozen solutions (Figure S28) gave EPR spectra typical of Cu^{II} complexes, with $g_{\perp} < g_{||}$ and a four-line hyperfine splitting around $g_{||}$ characteristic of the copper nucleus (⁶³Cu, 69.17%, $g_{\rm N} = 1.484$, I = 3/2, ⁶⁵Cu, 30.83%, I = 3/2, $g_{\rm N} = 1.5877$). The spectral parameters of the complexes were determined by simulation and found to be similar for all three complexes (Table S5). A trend in $g_{||}$ values was determined with CuL^H<

CuL^{CI} < CuL^{NO2} (Table 1), which corresponds to a decrease in splitting between the d_{xy} and $d_{x^2-y^2}$ orbitals (Δ_1) of the Cu^{II} centre, [32] and is in agreement with the UV/Vis absorption data. Partially resolved spectral features around q_{\perp} indicate contributions from hyperfine interactions with both the Cu centre and N atoms (^{14}N , I=1, 99.63%) of the CF₃PAPX ligands. Roomtemperature EPR measurements of the CuL^x complexes also were made, after 0 min and 24 hours of incubation at 37 °C (Figure S27). The resulting isotropic spectra were well simulated using the average of the frozen-solution g values: $g_{\rm iso} =$ (2 $g_{\perp} +$ $g_{||}$)/3; and copper hyperfine splitting of $A_{\rm iso}^{\rm Cu} =$ 66–77 G. This demonstrates that there is no significant conformational difference of the CuL^X complexes in liquid or frozen solutions. Furthermore, the spectra were unchanged after 24 hours, both in appearance and intensity, demonstrating that no additional ligand exchange occurs.[19]

As described above, the complexes CuL^x are stable in aqueous solution following initial acetate ligand loss. However, in vitro and in vivo environments provide an array of nucleophiles that could potentially be competitor ligands for Cu^{II} complexes. This was assessed by evaluating the stability of CuL^{NO2} in Dulbecco's modified Eagle's medium (DMEM), which was used to culture HeLa cervical adenocarcinoma cells in experiments described below. Limits on the aqueous solubility of CuL^{NO2} prevented studies of speciation by UV/Vis via analysis of d-d transitions. However, the CF₃ group of CF₃PAPXNO₂ enabled evaluation of coordination using ¹⁹F NMR. A 1:1 DMEM/DMSO solution was used in these studies to improve the solubility of CuLNO2 and prevent precipitation of free CF₃PAPXNO₂. CuL^{NO₂} exhibits a broad peak (FWHH=21 Hz) at -61.13 ppm, whereas the free ligand CF₃PAPNO₂ was detected at -61.06 ppm with a narrower linewidth (FWHH=6 Hz; Figure S21). The increased linewidth observed for the complex reflects the paramagnetic relaxation enhancement effect of the coordinated Cu^{II} ion.^[28a,33] Similar measurements in pure DMSO for chemical reduction studies, confirm these assignments (see below). CuL^{NO2} was incubated for up to 24 hours at 37 °C in 1:1 DMEM:DMSO and no change in the signal from the complex was observed, nor was any free ligand detected (Figure S21). This demonstrates that CuLNO2 is stable towards exchange of the tridentate CF₃PAPNO₂ ligand in the growth medium, indicating sufficient stability also in the biological studies described in this work.

Electronic properties

The CF₃PAPX ligands of the CuL^X complexes were modified at the *para* position of their phenol groups to both maximize the

Table 1. Summary of the electronic properties, cytotoxicity, and intracellular copper content of each CuL ^x complex under different experimental conditions.								
Complex	Electronic properties Hammett parameter ($\sigma_{\rm p}$)	d-d $\lambda_{\rm max}$ [nm] DMSO	g MES buffer	E _{Pc} [mV]	IC ₅₀ [μM] Normoxia	Hypoxia	Intracellular Cu o Normoxia	ontent [fmol/cell] Hypoxia
CuL ^H CuL ^{CI} CuL ^{NO} ₂	0 0.23 0.78	663 665 676	2.253 2.255 2.259	-790 -660 -560	50 ± 10 25 ± 10 25 ± 3	26±9 26±5 16±2	$\begin{array}{c} 0.15 \pm 0.01 \\ 0.267 \pm 0.007 \\ 1.5 \pm 0.1 \end{array}$	$\begin{array}{c} 0.26 \pm 0.03 \\ 0.53 \pm 0.04 \\ 3.0 \pm 0.2 \end{array}$



range of their reduction potentials and to locate them in the appropriate range for hypoxia selectivity. Cyclic voltammetry was performed for each CuL^x complex in MES buffer (Figure S30, Table 1) with 10% DMSO to improve aqueous solubility. Each CuL^x complex exhibited an irreversible wave between -560 and -790 mV vs. NHE. The low solubility of the ligands, along with the fast ligand exchange rate of Cu^1 , are likely contributors to the irreversibility of the reduction process. The cathodic peak potentials (E_{Pc}) decrease across the series, with $CuL^{NO_2} > CuL^{Cl} > CuL^{H}$. This correlates with the Hammett parameters (G_p)^[34] of the *para*-position substituents (Table 1) where the NO_2 derivative has the most electron-poor phenol and the H derivative presents the most electron-rich phenol.

To put the reduction potentials of CuL^X in context, the benchmark Cu^{II} hypoxia probe CuATSM has $E_{1/2} = -555 \text{ mV}$ versus Ag/AgCl^[17a] in a buffer/DMSO mixture at pH 6, which is approximately -356 mV vs. NHE.[35] Due to the irreversibility of our systems, the E_{Pc} of -590 mV (-391 mV vs. NHE) for CuATSM is a more appropriate comparison. Each of the CuL^x complexes have lower reduction potentials than CuATSM, suggesting that they could all be used as hypoxia-selective agents. The intracellular reduction potential of healthy cells is typically between -200 and -300 mV vs. NHE.^[36] Whereas, for example, in A549 non-small-cell lung cancer cells the intracellular redox status changed from -320 mV vs. NHE in normoxia to less than -420 mV in cells incubated in a hypoxic environment. [37] In general, the reduction potentials of CuL^X are lower than reported intracellular normoxia and hypoxia reduction potentials in cancer cells^[36c,37] as well as those of common biological reductants.[38] Initially, this suggested that these compounds could be challenging to reduce in biological hypoxic environments. To further examine the reduction of these compounds we thus undertook chemical reductions monitored by ¹⁹F NMR, UV/Vis, and EPR spectroscopy.

Reductive reactivity

Initially, chemical reductions were studied by UV/Vis in DMSO using the strong reducing agent sodium dithionite (Na₂S₂O₄, NaDT) to ensure complete reduction of the Cu^{II} centre.^[39] The addition of increasing equivalents of NaDT caused a corresponding decrease in the d-d transition band of each compound, as a result of reduction from Cu^{II} to Cu^I (Figure S24). The CF₃ group of the CF₃PAPX ligands allowed the redox processes of CuL^X to be studied through both ¹⁹F NMR and MRI (Figure 2). Similar to the stability studies described above, in DMSO the free CF₃PAPNO₂ ligand has a sharp ¹⁹F resonance (FWHH= 2.8 Hz) at -60.4 ppm, whereas the CuL^{NO_2} complex has a resonance at -60.6 ppm that is much broader (FWHH=44 Hz) due to the effect of paramagnetic relaxation enhancement from the Cu^{II} centre (Figure 2a). [28a,33] Similar ¹⁹F NMR spectra were observed for each CF₃PAPX ligand and CuL^X complex, with coordination to the Cu^{II} centre resulting in a shift of up to -0.2 ppm, and an increase in linewidth of 38-41 Hz. Details of relevant NMR properties for each CF₃PAPX ligand and CuL^X complex are given in Table S4.

To examine species that could potentially be generated under hypoxic conditions, a series of chemical reductions using NaDT were performed and characterized by ¹⁹F NMR (Figures 2a, S22, and S23). When reductions were carried out in aqueous solution, a decrease in the ¹⁹F NMR signal intensity from the Cu^{II}

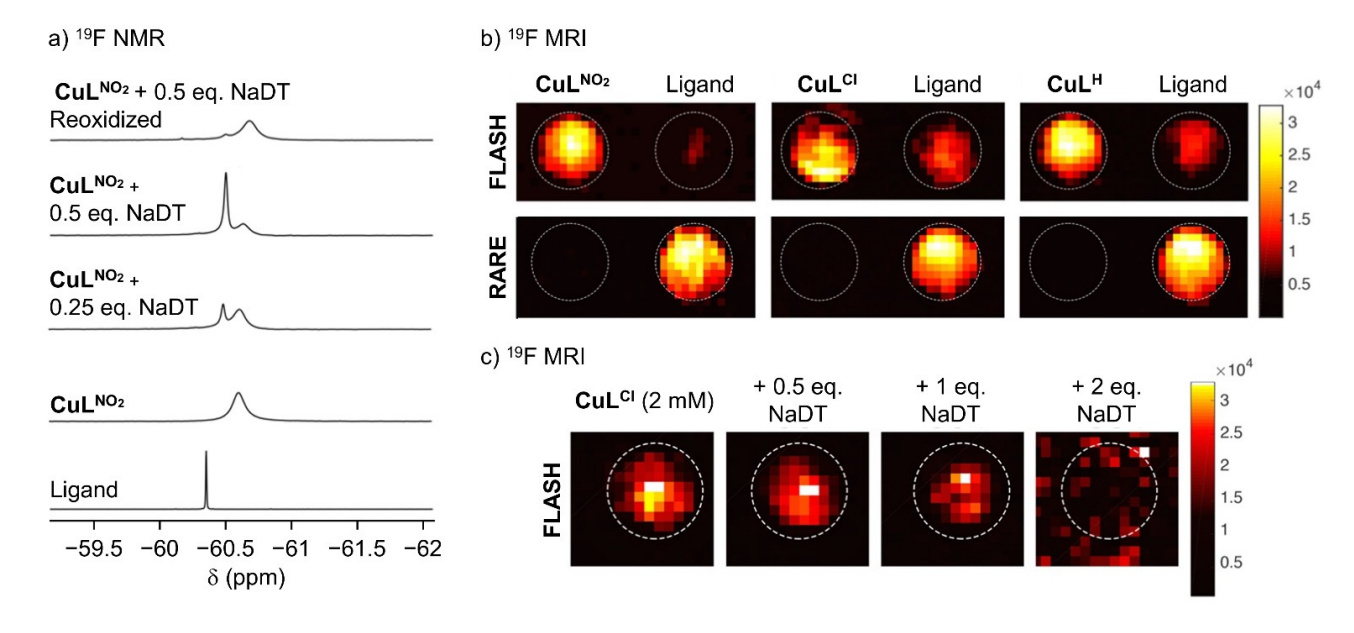


Figure 2. Left: a) 19 F NMR spectra of CF₃PAPNO₂ and CuL NO_2 in [D₆]DMSO, demonstrating the effect of coordination to the paramagnetic Cu^{II} centre on the appended fluorine atoms, and the spectra of the chemical reduction of CuL NO_2 by NaDT in DMSO. Each sample was prepared separately in an anaerobic chamber to prevent reoxidation. Right: Coronal MRI scans collected on each CF₃PAPX ligand and CuL X complex demonstrating the suitability of these compounds for study by 19 F MR methods. b) Two 500 μL Eppendorf tubes containing 4 mM CF₃PAPX in DMSO (right), and 4 mM CuL X in MES buffer (left). CuL X was best imaged by using the FLASH pulse sequence; CF₃PAPX was best imaged by using the RARE pulse sequence. c) The reduction of a 2 mM solution of CuL C in MES buffer (pH 6.5) with addition of 0.5, 1, and 2 equiv. of NaDT, detected using FLASH. All experiments were conducted at room temperature.



complexes was observed, but no new signals were detected. This indicates generation of Cu¹ complexes, leading to rapid release of the CF₃PAPX ligands, which then immediately precipitate. Similar behaviour has been reported for some CuATSM complexes.^[22] To mitigate this solubility issue, chemical reductions were carried out in DMSO. Anaerobic conditions were also used, to prevent reoxidation. Taking CuLNO2 as an example, addition of 0.25 equivalents of NaDT to the solution of CuL^{NO2} caused partial attenuation of the signal from the Cu^{II} complex and generated a new peak at -60.4 ppm (Figure 2a). Interestingly, the new signal has a different chemical shift and linewidth from either the Cu^{II} complex or the free ligand. Given the lability of Cu^I species, [40] the new peak likely reflects a fast exchange between the Cu^I complex and uncoordinated ligand, which is not resolved on the NMR timescale. Upon exposure to air the ¹⁹F signal from the Cu^{II} complex was regenerated (Figure 2a), demonstrating the reversibility of the reduction when the solvent system is suitable to prevent ligand precipitation. The ¹⁹F NMR studies thus demonstrate that MR methods are sensitive probes of the copper oxidation states in the CuL^x therapeutic candidates.

Although NaDT was used in these studies and the MRI experiments below to completely reduce the complexes, EPR measurements reveal that the milder reducing agent sodium ascorbate (NaAsc) can also reduce CuL^{NO2}. Incubation of the complex in MES buffer (pH 6.5) at room temperature with NaAsc results in attenuation of the EPR signal from the complex, demonstrating reduction of the paramagnetic Cu^{II} species to diamagnetic Cu^{II} (Figure S29). Significantly, this shows that CuL^{NO2} can be reduced by biological reducing agents, and thus can be activated in cells/in vivo.

¹⁹F MRI

Recent studies have demonstrated the use of ¹⁹F MRI-based methods to study the reduction of Cu^{II} complexes, allowing differentiation of both oxidized and reduced forms. ^[18b] In this work, we applied ¹⁹F MRI to probe the CuL^X complexes and their corresponding ligands under reducing conditions. A series of phantom images were acquired on a 7 T preclinical MRI.

Each of the ligands has a longitudinal relaxation time (T_1) of 0.97–1.00 s and a transverse relaxation time (T_2) of 0.69–0.75 s, consistent with a diamagnetic species. Complexation of the paramagnetic Cu^{\parallel} ion decreased the T_1 and T_2 values to between 9.3-10.4 and 6.6-7.6 ms, respectively. These differences in relaxation times enabled selective imaging of CF₃PAPX or CuL^X. The fast low-angle shot (FLASH)^[41] pulse sequence with a short repetition time (TR, <6 ms) and short echo time (TE, 1.17 ms) was used to selectively image the fast-relaxing paramagnetic Cu^{II} complexes (Figure 2b); under this short TR setting, the slow-relaxing CF₃PAPX ligand signals are mostly saturated. On the other hand, the rapid acquisition with relaxation enhancement (RARE)[42] pulse sequence with a long TE (100 ms) and a moderate TR (1.5 s) was used to selectively image the diamagnetic CF₃PAPX ligands (Figure 2b). In this case the long echo ensures the ¹⁹F nuclear spin polarization of the Cu^{II}

complexes return to thermal equilibrium prior to acquisition, resulting in no detected signal. The shorter TR used for imaging the Cu^{II} complexes also allows more imaging replicates per unit time, giving a higher imaging signal-to-noise ratio (SNR) than the ligand measurements. As shown in Figure 2b and Table S6, the Cu^{II} complexes had a 2- to 3.8-fold higher SNR than that of their corresponding ligands at the same concentration.

To demonstrate ¹⁹F MRI detection of CuL^X reduction, we imaged CuL^{CI} in MES buffer (pH 6.5) in the presence of increasing equivalents of NaDT (Figure 2c). As shown in Figure 2c, by employing the FLASH sequence, which is specific for the Cu^{II} complexes, an intense signal was detected from CuL^{CI}. Addition of NaDT leads to a decrease in signal intensity, with essentially complete attenuation achieved with 2 equivalents of the reducing agent. Similar behaviour was observed for all of the CuL^X complexes (Figure S31). These results demonstrate the utility of the MRI method to study changes to the oxidation state of the Cu species under physiological conditions. However, the low aqueous solubility of the free CF₃PAPX ligands meant they were not detected readily in MES buffer. In more complex biological systems, such as in vivo, biomolecule interactions are expected to increase the solubility of the ligand, potentially allowing RARE imaging of the reduced species.

Analysis of therapeutic potential

The cytotoxicity of the CuL^X complexes was evaluated in HeLa cervical adenocarcinoma cancer cells using standard MTT protocols (Table 1). IC₅₀ values were determined after 24 hours of exposure to the complexes under both normoxic (5% CO₂, $20\,\%$ $\,O_2)$ and hypoxic (5 % $\,CO_2,~0.1\,\%$ $\,O_2)$ conditions (Table 1, Figure 3a). Under normoxic conditions, CuL^{NO2} and CuL^{CI} have the same IC_{50} values of 25 μM . CuL^{H} , the complex with the lowest reduction potential, had the highest IC₅₀ (50 μ M). When the complexes were assayed under hypoxic conditions, both CuL^H and CuL^{NO2} exhibited significantly enhanced cytotoxicity with IC₅₀ values of 26 and 16 μM respectively. CuL^{CI} had no significant difference in cytotoxicity between the normoxic and hypoxic assays. While these results do not show a direct relationship to the reduction potentials of each of the complexes, the enhanced activity of both CuL^H and CuL^{NO2} in hypoxia suggests the potential for selectivity towards hypoxic environments. Furthermore, CuLNO2, which has the highest reduction potential, exhibits the highest cytotoxicity in both normoxic and hypoxic conditions, suggesting that the CuL^H and CuL^{CI} complexes may have reduction potentials too low for optimal biological activity. The cytotoxicity of the ligands was not determined due to their low aqueous solubility.

To gain deeper insight into the mechanisms of metabolic inhibition, we performed fluorescence microscopy analysis of HeLa cells incubated with CuL^{NO_2} (20 μM), under both hypoxic and normoxic conditions, using Hoechst 33342 stain (cell membrane permeable, giving total cell count) and propidium iodide (PI, cell membrane impermeable) nuclear stains (Figures 4a and S32). Comparing the tested and control cells, higher CuL^{NO_2} cytotoxicity was observed in hypoxia with a calculated



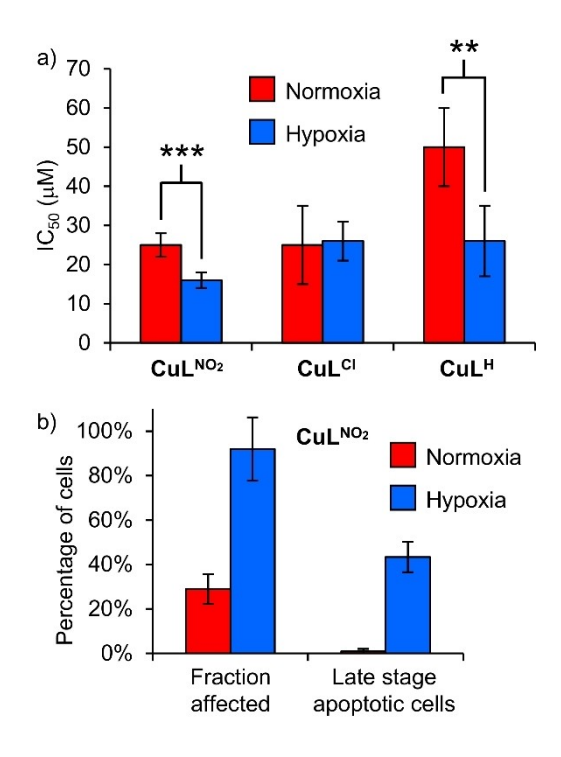


Figure 3. Results of cytotoxicity studies of CuL^x with HeLa cells. a) IC₅₀ values for each CuL^X complex as determined by MTT assay. b) Analysis of the effects of 20 $\mu M \; \text{CuL}^{\text{NO}_2}$ on HeLa cells evaluated by using Hoechst and PI staining and image analysis with ImageJ. **p < 0.005, ***p < 0.001.

 $93\pm14\%$ fraction affected, while only a $29\pm7\%$ fraction affected was seen under normoxic conditions (Figure 3b). Treatment with CuL^{NO2} under hypoxia also strongly affects cell morphology, producing abnormally rounded cells, with many cells exhibiting rounded and condensed nuclear matter (Fig-

Incubation with CuL^{NO2} in hypoxic conditions resulted in $43\pm7\%$ of cells co-stained by PI and Hoechst dyes, indicating either necrosis or late-stage apoptosis. [43] However, many cells with abnormal whole-cell and nuclear morphology were stained only by the Hoechst dye. This abnormal morphology and absence of PI staining indicates apoptosis, suggesting that the cells that have been co-stained are undergoing late-stage apoptosis rather than necrosis.[43] In contrast, in normoxic environments only $1\pm1\,\%$ of cells were in late-stage apoptosis (co-stained) following treatment with CuL^{NO_2} .

Nuclear condensation, characteristic of apoptosis, can be quantified by the average size of all nuclei as visualized by the Hoechst stain. [44] In the absence of CuLNO2, the average nuclear size was $270 \pm 70 \,\mu\text{m}^2$, with no significant difference observed between the nuclei in normoxic and hypoxic environments (Figure 4b). When CuL^{NO2} was introduced under normoxic conditions, an average nuclear size of $230\pm40~\mu\text{m}^2$ was observed, indicating a slight, not statistically significant contraction. However, under hypoxic conditions, CuLNO2 caused the average nuclear size to shrink to $150\pm10\,\mu\text{m}^2$, which is significantly smaller than the nuclei of the control wells (p < 0.001), and is a characteristic morphological sign of apoptosis (Figure 4b). [45] This quantifiable nuclear condensation further

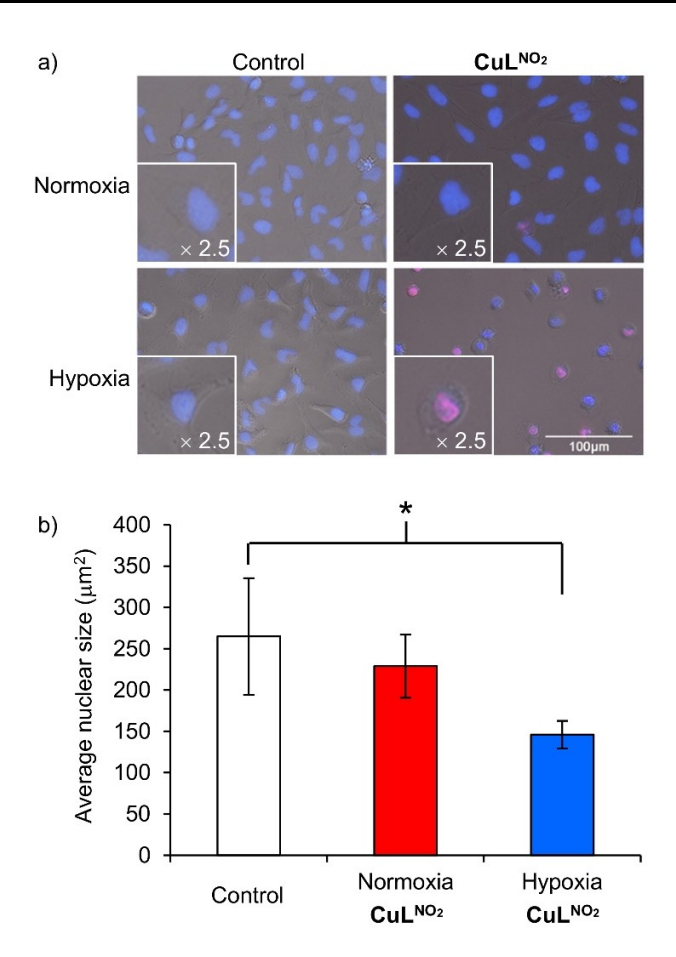


Figure 4. a) HeLa cells incubated with and without CuL^{NO_2} under both normoxic and hypoxic conditions. Cells were incubated with either a DMSO vehicle control or with CuL^{NO2} for 24 h, and then stained with Hoechst 33342 (blue) as a cell membrane-permeable dye and propidium iodide (red) as a cell membrane-impermeable stain. Imaged at 40× magnification. b) Analysis of the nuclear morphology indicates a significant contraction when cells are incubated with CuLNO2 under hypoxic conditions. Nuclear size was determined by using Hoechst staining, and analysed by determining particle size in ImageJ with $10 \times$ images. Control: N = 2332 nuclei; normoxia CuL^{NO2}: N=2010 nuclei; hypoxia CuL^{NO2} N=319 nuclei. *p<0.001.

supports the hypothesis that CuLNO2 induces apoptosis, rather than necrosis, and does so under hypoxic conditions but not normoxic conditions.

Cell uptake

In addition to enhancement of cytotoxicity under hypoxic conditions, another desirable property of selective anticancer agents is increased uptake by cells under hypoxia. The cellular uptake of the CuL^x complexes was evaluated by determining the intracellular copper content (Table 1) using inductively coupled plasma optical-emission spectrometry (ICP-OES). HeLa cells were prepared for these measurements by incubation with 20 µM solutions of each complex for 4 hours under hypoxic and normoxic conditions (Figure 5a, Table 1). The uptake in normoxia was low to moderate for each CuL^X complex (0.15–1.5 fmol/ cell) compared, for example, to the uptake of fluorinated



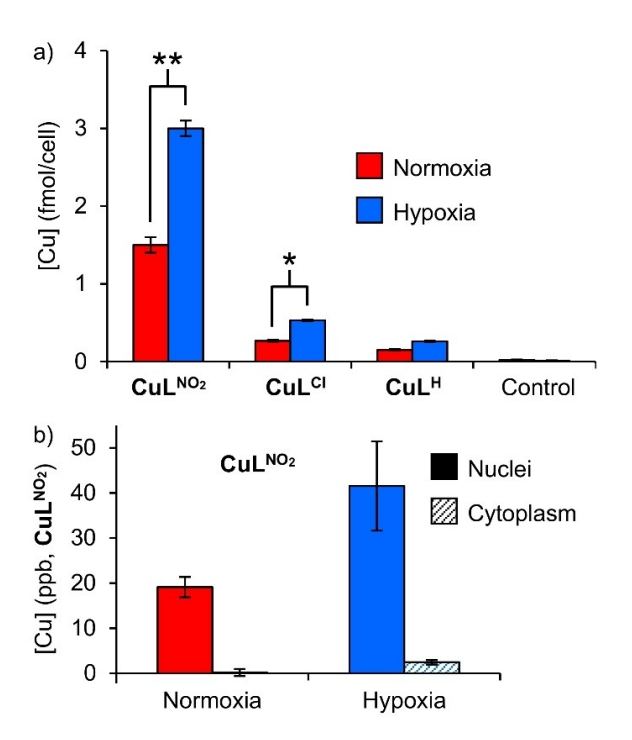


Figure 5. Cellular copper uptake, and subcellular fractionation studies of CuL^x with HeLa cells. a) Cellular copper uptake of each of the compounds incubated with HeLa cells at 20 μM for 4 h. b) Nuclear and cytoplasmic copper concentrations in HeLa cells following incubation with 20 $\mu M \; \text{CuL}^{NO_2}.$ ** p < 0.001, * p < 0.005.

CuATSM derivatives. [18a] However, all of the compounds had enhanced uptake under hypoxia, with intracellular copper content ranging from 0.26 to 3.0 fmol/cell depending on the complex (Table S8). Notably, the most active compound, CuL^{NO2}, also demonstrated the greatest uptake enhancement under hypoxic conditions, with an increase of at least twofold in the intracellular copper concentration (3.0 \pm 0.2 fmol/cell).

Previous studies have correlated differences in cellular metal-based anticancer compounds uptake of lipophilicity.^[46] To establish if this was a factor in the relative intracellular accumulation of the CuL^X complexes, their lipophilicities were evaluated using the shake-flask method. [47] The $\log p$ values of the complexes fell within a small range: -0.05 < $\log p < 0.37$, (Table S9), thus indicating that this is not a major factor in their cellular accumulation.

To gain more insight into the transport processes for CuL^{NO₂} the complex was also incubated with HeLa cells at 4°C for 4 h (Figure S34, Table S8). At the lower temperature the cells exhibited a small but significant (p < 0.001) increase in Cu content compared to 37° C (3.9 ± 0.2 vs. 3.0 ± 0.2 fmol/cell). These data suggest an energy-independent uptake mechanism such as passive or facilitated diffusion. [48] Similar results of increased uptake upon metabolic inhibition were observed for a ruthenium(II) polypyridyl compound, where the authors suggest that this is likely the result of reduced efflux.[49] Thus, one possible interpretation of these data is that CuL^{NO_2} is imported passively but actively exported across the cellular membrane. However, the effects of chaperones and changes in speciation equilibria with temperature might also be involved.

Taken together, these observations indicate the importance of cell uptake studies to the cytotoxic mechanism of CuL^X. The intracellular Cu content increased according to CuL^{NO2} > CuL^{Cl} > CuL^H, matching the ordering of the Hammett parameter values of the functional groups. One possible explanation for this is that the para-position substituents modulate the ligand affinity for Cu²⁺ as the acidity of the phenol increases. Thus, the CuL^{NO₂} complex is more likely to remain intact following cellular uptake through passive pathways, allowing for Cu accumulation without ligand dissociation. Loss of CF₃PAPX ligands from the complexes will result in free Cu^{2+} ions, which are tightly regulated by the cell and would be rapidly taken up by relevant chaperones, before being effluxed through active pathways. [50] Therefore, the CF₃PAPNO₂ ligand of CuL^{NO₂} likely is responsible for a greater intracellular Cu concentration, which in turn contributes in part to greater cytotoxic activity.

Subcellular localization

To gain additional insight into the mechanism of action of CuL^{NO2}, subcellular fractionation was used to probe localization of the complex in the cytoplasm or nuclei of HeLa cells. The cells were incubated with CuLNO2 and fractionated into nuclear and cytoplasmic fractions according to the "rapid, efficient and practical" (REAP) protocol,[51] with subsequent analysis by ICP-OES (Figure 5b). Significantly, under both atmospheres the intracellular copper was found to be almost exclusively located in the nuclei and not in the cytoplasm. Furthermore, approximately twice as much Cu was found in the nuclei under hypoxic conditions. These results, combined with the nuclear morphologies characterized by Hoechst staining (see above), suggest that the cytotoxicity of these complexes is caused by interactions with nuclear targets, such as DNA or nuclear proteins, leading to apoptosis.

Although the ICP-OES measurements demonstrate that exposure to CuLNO2 generates elevated Cu concentrations in HeLa-cell nuclei, the status of the CF₃PAPX ligands is also extremely important. The presence or absence of functional ligands is central to the mechanism of many metal-based anticancer compounds since they modulate transport processes, biomolecule interactions, and reduction potentials. [9b,12b,17b,52] These considerations are particularly important for Cu-based metallodrugs given the sensitivity of the reduction potential of the metal centre to the ligand environment, and the lability of Cu^{II} and Cu^{II} species. Previous approaches to this problem have included XAS measurements of iodine-labelled Ru^{III} anticancer complexes,^[53] the study of photoactive compounds in cells, [48,54] and the application of imaging mass spectrometry. [55] The CF₃ spectroscopic handle of CuLNO2 enabled the use of 19F NMR to assess intracellular localization. To our knowledge this is the first example of this approach to chemotherapeutics. HeLa cells were prepared for these studies by incubating with 20 µM CuL^{NO2} for 4 hours under normoxic conditions and fractionated. The compounds



were then extracted with DMSO for ^{19}F NMR analysis (Figure 6). The whole-cell fraction and the nuclear fraction gave a single ^{19}F resonance at -60.4 ppm, whereas the cytoplasmic fraction had no signals. The linewidth and peak shape of the signal from the nuclear fraction and whole cells match with that of the CF_3PAPNO_2 ligand in $[D_6]DMSO$. To confirm the identity of this species, an aliquot of CF_3PAPNO_2 in DMSO was added to the whole-cell fraction, and the signal intensity at -60.4 ppm increased (Figure 6).

These experiments demonstrate the utility of ¹⁹F NMR for detecting CF₃-modified ligands in cells. In this case, the fractionation workup likely causes dissociation of the CF₃PAPNO₂ ligand and so this method does not directly characterize the complete CuL^{NO₂} complex. However, combining these observations with the ICP-OES data demonstrates that the copper ion and CF₃PAPNO₂ ligand are co-localized in the nucleus. This is indirect evidence for CuL^{NO₂} being transported intact but is consistent with the solution stability studies described above.

DNA interactions and reactions

To probe the interactions of CuL^{NO_2} with nucleic acids, UV/Vis studies with calf-thymus DNA (ctDNA) were performed in MES buffer (pH 6.5). A 50 μ M solution of CuL^{NO_2} gave a λ_{max} at 378 nm with an absorbance of 0.665 AU. When 10 equiv. of ctDNA was added to this solution, there was a small reduction in the absorbance intensity (0.650 AU, ~2% change) and no change in the λ_{max} wavelength (Figure S26). This contrasts with

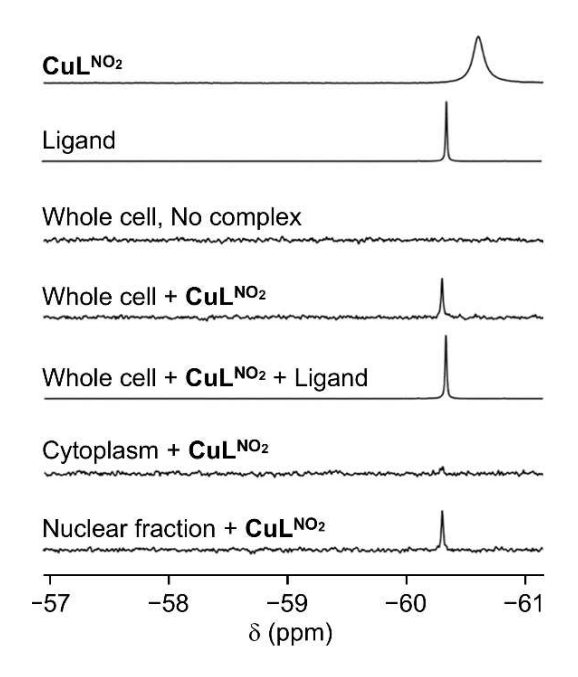


Figure 6. ¹⁹F NMR spectra of CuL^{NO2} cellular localization. From top to bottom: reference spectra of CuL^{NO2} and CF₃PAPNO₂ ligand in DMSO; whole HeLa cells without complex added; whole HeLa cells after incubation with CuL^{NO2} for 4 h;; whole HeLa cells incubated with CuL^{NO2} and subsequently spiked with CF₃PAPNO₂ ligand; cytoplasmic and nuclear fractions from HeLa cells incubated with CuL^{NO2}.

known Cu^{II} complex-based DNA intercalators^[17c,52c,56] that exhibit significantly stronger hypochromism (9–20%) in addition to shifts in λ_{max} by 1–3 nm in their UV absorption band when incubated with ctDNA. Furthermore, addition of a stronger-field ligand, such as nitrogen from a nucleotide, in place of water or hydroxide in the fourth equatorial-coordination site of CuL^{NO2}, is predicted to give a blue shift.^[57] Thus, these data suggest that the complex does not interact strongly with DNA by either intercalation or coordination.

The potential effect of CuLNO2 on DNA was also characterized using agarose gel electrophoresis studies of pet22b plasmids. Incubation of the compound alone (1-100 equiv., Figure 7a) in MES buffer (pH 6.5) with the DNA had no effect on plasmid migration through the gel. This confirms that neither intercalation nor copper-DNA coordination are likely to be significant factors in the activity of the compound. Cull complexes are established chemical nucleases capable of cleaving DNA, particularly in the presence of reducing agents. [52b,58] To determine if CuL NO2 could generate redoxdependent DNA damage, the complex was incubated with the plasmid and increasing equivalents of NaAsc (0-50 equiv., Figure 7b). This led to a transformation of the DNA from the native supercoiled form (SC) to the linear form (L) and was dependent on the concentration of the reducing agent. Observation of the linear form of the plasmid demonstrates double-strand breaks, as opposed to single-strand breaks leading to the open-circular (OC) form, and is consistent with the possible effects of ROS generation by CuLNO2 following reduction.[12b,56] This shows that CuLNO2 can be activated by biological reducing agents to cleave DNA, which could then lead to apoptosis. The requirement for a reducing agent to initiate this process also suggests the origin of the selective activation of in vitro cytotoxicity under hypoxic conditions.

Conclusions

We have developed a series of ¹⁹F-tagged copper pyridine aminophenolate-based complexes (CuL^X) that function both as hypoxia-activated cytotoxins and MR probes. Although the

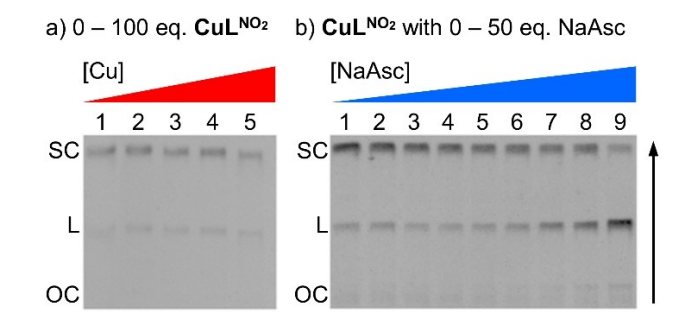


Figure 7. Electrophoresis studies of pet22b DNA plasmid and CuL^{NO}₂. Each lane contains 10 μM DNA; samples were incubated for 1 h at 37 °C in MES buffer (pH 6.5). a) Lane 1: DNA only; lanes 2–5: 10, 100, 500 and 1000 μM CuL^{NO}₂. b) Lane 1: DNA only; lane 2: 125 μM sodium ascorbate; lanes 3–9: 2.5 μM CuL^{NO}₂ and 0, 1.25, 2.5, 5, 12.5, 25, and 125 μM sodium ascorbate.



potential for Cu^{II} complexes to selectively target hypoxia for cytotoxic activation has been widely discussed, it has only rarely been demonstrated.^[59] In addition, we present one of the first reports of Cu^{II}-based hypoxia-activated imaging not based on the Cu^{II} ATSM scaffold.^[60]

The origin of the cytotoxicity exhibited by many Cu^{II} complexes has been linked to an initial reduction step to give Cu¹ species, which then generate ROS by redox cycling of the metal centre through Fenton-like chemistry. [12b,17c,52b] With this in mind, substitution at the para position of the phenol in the CF₃PAPX ligand backbone was used to tune the reduction potential of the Cu^{II}/Cu^I couple of the CuL^X compounds. These modifications varied the potentials over a range of 200 mV, with a trend that was in accordance with the corresponding Hammett parameters. The reduction potentials of all three CuL^X complexes are below the anticipated window for hypoxic tissues, and thus well below that found in normoxic environments. Consequently, these compounds have the potential to demonstrate selective hypoxic activation. Based on the IC₅₀ values determined against HeLa cells in both hypoxic and normoxic environments, the reduction potentials of the H- and Cl-substituted complexes were too low to exhibit cytotoxicity selectivity. However, the NO_2 -substituted complex, with E_{Pc} = -560 mV, had a reduction potential both high enough to potentially undergo reduction by biological systems and low enough that its activity was selective for hypoxic cells.

Enhancement of copper accumulation is another property of the CuL^X complexes that promotes hypoxia selectivity. ICP-OES studies of HeLa cells following exposure to CuL^x show a twofold increase in copper concentration under hypoxic versus normoxic conditions. Significantly, CuLNO2 shows much greater overall accumulation than the other complexes, likely contributing to the higher general cytotoxicity and particularly the hypoxia-selective cytotoxicity of this compound. In cellular environments copper homeostasis is tightly regulated, [50] with excess copper exported by transport proteins such as Atox1. [61] Copper transporters contribute to cisplatin resistance in several cancers and they present an on-going challenge to the application of metal-based therapeutics.^[62] Retention of ligands by copper complexes following transport into cells could play a role in reducing export by copper-transport proteins leading to higher intracellular Cu concentrations. The electron-withdrawing NO₂ group is expected to increase the acidity of the CF₃PAPNO₂ phenol, potentially stabilizing coordination to Cu^{II}, and thus promoting retention of CuL^{NO2} following transport into HeLa cells.

Subcellular fractionation analyses by ICP-OES, following incubation of HeLa cells with CuL^X show elevated copper concentrations in cell nuclei, but no significant accumulation in the cytoplasm. Observation of nuclear targeting suggests a role for the CF₃PAPX ligands in both the transport and localization of copper ions. This hypothesis is supported by ¹⁹F NMR studies of CuL^{NO2}, which show that the CF₃PAPNO₂ ligand also localizes in the nucleus. This is encouraging, but indirect, evidence for the complex being transported with the ligand bound within cells. Furthermore, ¹⁹F NMR studies of CuL^{NO2} in cell growth medium (DMEM) show that the tridentate CF₃PAPNO₂ ligand

remains coordinated to the Cu^{II} ion even after 24 hours of incubation at 37 °C. Consequently, we anticipate that CuL^{NO_2} is sufficiently stable to act concertedly in a biological environment.

Hypoxia-selective nuclear localization is consistent with a cytotoxicity mechanism involving ROS-dependent DNA damage. DNA nuclease activity of CuL^{NO2} was demonstrated by plasmid cleavage in the presence of the biologically-relevant reducing agent sodium ascorbate. Such activity in HeLa cells is expected to promote cell death according to an apoptosis pathway, and this was confirmed for CuL^{NO2} by fluorescence imaging studies.

In addition to hypoxia-selective transport and cytotoxicity, we demonstrate that, by including a CF₃-functionalized pendant arm as part of the CF₃PAPX ligand scaffold, the CuL^X complexes can function as ¹⁹F NMR and MRI probes. The proof-of-principle ¹⁹F MRI studies show that the different relaxation times of the diamagnetic ligands and paramagnetic complexes can be used to characterize reduction processes through the application of two different MRI pulse sequences. These experiments show that this approach can differentiate the free ligand, and potentially also Cu^I systems, from paramagnetic Cu^{II} species. Exploitation of this 19F MRI method, when applied in conjunction with traditional ¹H MRI, could provide in vivo spatial evaluation of the tumour localization of these types of compounds. Simultaneously, redox status could be determined, providing analysis of the pharmacological behaviour of the complexes in real time. [26b]

Overall, we have shown that the properties of Cu^{II} complexes can be tuned through ligand design for hypoxia-selective cytotoxicity and MR imaging. In this case, selection of a ligand scaffold, CF₃PAPX, that can be constructed by modular synthesis, readily accessed a range of reduction potentials while also providing a ¹⁹F spectroscopic handle. Furthermore, the lead compound, CuL^{NO2}, shows both hypoxia-selective cytotoxicity and cellular accumulation. This demonstrates an additional dimension for the optimization of redox-active metal-based anticancer cytotoxins with reduced side effects.

Acknowledgements

We acknowledge the Imaging Research Center and Dr. Jonathan Sessler for access to the MRI facilities and the microplate reader, respectively. Dr. Tim Storr (Simon Fraser University) is acknowledged for useful discussions of the electrochemical data, and Dr. Jeffrey Warren (Simon Fraser University) for access to electrochemical facilities. The work carried out at Simon Fraser University was supported by funding from the Natural Sciences and Engineering Research Council of Canada (NSERC) to C.J.W. (RGPIN312575), and the work at the University of Texas at Austin was supported by funding from the Welch Foundation (F-1883) and National Science Foundation (NSF, CHE-1945401) to E.L.Q.. K.E.P. acknowledges financial support provided through an NSERC Vanier Canada Graduate Scholarship, and the Michael Smith Foreign Study Supplement.



Conflict of Interest

The authors declare no conflict of interest.

Keywords: cancer \cdot copper \cdot fluorine \cdot hypoxia \cdot magnetic resonance imaging

- [1] K. Hauner, P. Maisch, M. Retz, Der Urologe. Ausg. A 2017, 56, 472-479.
- [2] A.-M. Florea, D. Büsselberg, Cancers 2011, 3, 1351–1371.
- [3] T. M. Allen, Nat. Rev. Cancer 2002, 2, 750-763.
- [4] a) D. Liao, R. S. Johnson, Cancer Metastasis Rev. 2007, 26, 281–290;
 b) K. A. Kennedy, B. A. Teicher, S. Rockwell, A. C. Sartorelli, Biochem. Pharmacol. 1980, 29, 1–8.
- [5] K. Jung-whan, P. Gao, C. V. Dang, Cancer Metastasis Rev. 2007, 26, 291– 298
- [6] P. Vaupel, A. Mayer, Cancer Metastasis Rev. 2007, 26, 225-239.
- [7] a) N. Graf, S. J. Lippard, Adv. Drug Delivery Rev. 2012, 64, 993–1004;
 b) W. R. Wilson, M. P. Hay, Nat. Rev. Cancer 2011, 11, 393–410.
- [8] a) H. R. Mellor, S. Snelling, M. D. Hall, S. Modok, M. Jaffar, T. W. Hambley,
 R. Callaghan, *Biochem. Pharmacol.* 2005, 70, 1137–1146; b) M. D. Hall,
 H. R. Mellor, R. Callaghan, T. W. Hambley, *J. Med. Chem.* 2007, 50, 3403–3411.
- [9] a) A. Kellett, Z. Molphy, V. McKee, C. Slator, *RSC Metallobiol*. 2019, *14*, 91–119; b) C. Santini, M. Pellei, V. Gandin, M. Porchia, F. Tisato, C. Marzano, *Chem. Rev.* 2014, *114*, 815–862; c) L. Ruiz-Azuara, M. E. Bravo-Gomez, *Curr. Med. Chem.* 2010, *17*, 3606–3615.
- [10] N. K. Singh, A. A. Kumbhar, Y. R. Pokharel, P. N. Yadav, J. Inorg. Biochem. 2020, 210, 111134.
- [11] S. Adsule, V. Barve, D. Chen, F. Ahmed, Q. P. Dou, S. Padhye, F. H. Sarkar, J. Med. Chem. 2006, 49, 7242–7246.
- [12] a) C. A. Bolos, K. T. Papazisis, A. H. Kortsaris, S. Voyatzi, D. Zambouli, D. A. Kyriakidis, J. Inorg. Biochem. 2002, 88, 25–36; b) K. E. Prosser, S. W. Chang, F. Saraci, P. H. Le, C. J. Walsby, J. Inorg. Biochem. 2017, 167, 89–99; c) M. Devereux, D. O'Shea, A. Kellett, M. McCann, M. Walsh, D. Egan, C. Deegan, K. Kedziora, G. Rosair, H. Mueller-Bunz, J. Inorg. Biochem. 2007, 101, 881–892; d) S. Amer, N. El-Wakiel, H. El-Ghamry, J. Mol. Struct. 2013, 1049, 326–335.
- [13] a) S. Ramakrishnan, V. Rajendiran, M. Palaniandavar, V. S. Periasamy, B. S. Srinag, H. Krishnamurthy, M. A. Akbarsha, *Inorg. Chem.* 2009, 48, 1309–1322; b) K. Laws, G. Bineva-Todd, A. Eskandari, C. Lu, N. O'Reilly, K. Suntharalingam, *Angew. Chem. Int. Ed.* 2018, 57, 287–291; *Angew. Chem.* 2018, 130, 293–297.
- [14] a) S. Tardito, L. Marchio, Curr. Med. Chem. 2009, 16, 1325–1348; b) U. Jungwirth, C. R. Kowol, B. K. Keppler, C. G. Hartinger, W. Berger, P. Heffeter, Antioxid. Redox Signaling 2011, 15, 1085–1127.
- [15] V. Rajendiran, R. Karthik, M. Palaniandavar, H. Stoeckli-Evans, V. S. Periasamy, M. A. Akbarsha, B. S. Srinag, H. Krishnamurthy, *Inorg. Chem.* 2007, 46, 8208–8221.
- [16] B. M. Zeglis, V. Divilov, J. S. Lewis, J. Med. Chem. 2011, 54, 2391–2398.
- [17] a) Z. Xiao, P. S. Donnelly, M. Zimmermann, A. G. Wedd, *Inorg. Chem.* 2008, 47, 4338–4347; b) J. L. Dearling, J. S. Lewis, G. E. Mullen, M. J. Welch, P. J. Blower, *JBIC J. Biol. Inorg. Chem.* 2002, 7, 249–259; c) V. G. Vaidyanathan, B. U. Nair, *J. Inorg. Biochem.* 2003, 93, 271–276.
- [18] a) D. Xie, S. Kim, V. Kohli, A. Banerjee, M. Yu, J. S. Enriquez, J. J. Luci, E. L. Que, Inorg. Chem. 2017, 56, 6429–6437; b) D. Xie, T. L. King, A. Banerjee, V. Kohli, E. L. Que, J. Am. Chem. Soc. 2016, 138, 2937–2940; c) J. L. J. Dearling, P. J. Blower, Chem. Commun. 1998, 2531–2532; d) M. Yu, B. S. Bouley, D. Xie, J. S. Enriquez, E. L. Que, J. Am. Chem. Soc. 2018, 140, 10546–10552; e) J. S. Enriquez, M. Yu, B. S. Bouley, D. Xie, E. L. Que, Dalton Trans. 2018, 47, 15024–15030; f) A. Hino-Shishikura, U. Tateishi, H. Shibata, T. Yoneyama, T. Nishii, I. Torii, K. Tateishi, M. Ohtake, N. Kawahara, T. Inoue, Eur. J. Nucl. Med. Mol. Imaging 2014, 41, 1419–1427.
- [19] K. E. Prosser, C. J. Walsby, Eur. J. Inorg. Chem. 2017, 2017, 1573–1585.
- [20] B. Gallez, M. Swartz Harold, *NMR Biomed.* **2004**, *17*, 223–225.
- [21] a) N. Do Quyen, S. Ratnakar James, Z. Kovács, A. D. Sherry, ChemMed-Chem 2014, 9, 1116–1129; b) L. A. Basal, M. D. Bailey, J. Romero, M. Ali, L. Kurenbekova, J. Yustein, R. G. Pautler, M. J. Allen, Chem. Sci. 2017, 8, 8345–8350.
- [22] R. Maurer, P. Blower, J. Dilworth, C. Reynolds, Y. Zheng, G. Mullen, J. Med. Chem. 2002, 45, 1420–1431.
- [23] a) P. Porcari, S. Capuani, E. D'Amore, M. Lecce, A. La Bella, F. Fasano, R. Campanella, L. M. Migneco, F. S. Pastore, B. Maraviglia, *Phys. Med. Biol.*

- **2008**, *53*, 6979–6989; b) M. Yu, D. Xie, K. P. Phan, J. S. Enriquez, J. J. Luci, E. L. Que, *Chem. Commun.* **2016**, *52*, 13885–13888.
- [24] B. Condon, EPMA J 2011, 2, 403-410.
- [25] M. S. Fox, J. M. Gaudet, P. J. Foster, Magn. Reson. Insights 2015, 8, 53–67.
- [26] a) M. Oishi, S. Sumitani, Y. Nagasaki, Bioconjugate Chem. 2007, 18, 1379–1382; b) I. Tirotta, V. Dichiarante, C. Pigliacelli, G. Cavallo, G. Terraneo, F. B. Bombelli, P. Metrangolo, G. Resnati, Chem. Rev. 2015, 115, 1106–1129; c) A. M. Kenwright, I. Kuprov, E. De Luca, D. Parker, S. U. Pandya, P. K. Senanayake, D. G. Smith, Chem. Commun. 2008, 2514–2516; d) S. Mizukami, H. Matsushita, R. Takikawa, F. Sugihara, M. Shirakawa, K. Kikuchi, Chem. Sci. 2011, 2, 1151–1155; e) S. Mizukami, R. Takikawa, F. Sugihara, Y. Hori, H. Tochio, M. Wälchli, M. Shirakawa, K. Kikuchi, J. Am. Chem. Soc. 2008, 130, 794–795.
- 27] a) Q. Shi, Y. Li, S. Bo, X. Li, P. Zhao, Q. Liu, Z. Yang, H. Cong, H. Deng, M. Chen, S. Chen, X. Zhou, H. Ding, Z.-X. Jiang, Chem. Commun. 2016, 52, 5136–5139; b) C. Zhang, S. S. Moonshi, Y. Han, S. Puttick, H. Peng, B. J. A. Magoling, J. C. Reid, S. Bernardi, D. J. Searles, P. Král, A. K. Whittaker, Macromolecules 2017, 50, 5953–5963; c) K. J. Thurecht, I. Blakey, H. Peng, O. Squires, S. Hsu, C. Alexander, A. K. Whittaker, J. Am. Chem. Soc. 2010, 132, 5336–5337; d) X. Liu, Y. Yuan, S. Bo, Y. Li, Z. Yang, X. Zhou, S. Chen, Z. X. Jiang, Eur. J. Org. Chem. 2017, 2017, 4461–4468; e) S. Bo, Y. Yuan, Y. Chen, Z. Yang, S. Chen, X. Zhou, Z.-X. Jiang, Chem. Commun. 2018, 54, 3875–3878; f) J. Cui, R. Jiang, C. Guo, X. Bai, S. Xu, L. Wang, J. Am. Chem. Soc. 2018, 140, 5890–5894; g) Q. Peng, Y. Li, S. Bo, Y. Yuan, Z. Yang, S. Chen, X. Zhou, Z.-X. Jiang, Chem. Commun. 2018, 54, 6000–6003; h) J. Chen, M. Lanza Gregory, A. Wickline Samuel, Wiley Interdiscip. Rev. Nanomed. Nanobiotechnol. 2010, 2, 431–440.
- [28] a) R. B. Lauffer, Chem. Rev. 1987, 87, 901–927; b) J. Iwahara, C. D. Schwieters, G. M. Clore, J. Am. Chem. Soc. 2004, 126, 5879–5896.
- [29] a) P. S. Nadaud, J. J. Helmus, S. L. Kall, C. P. Jaroniec, J. Am. Chem. Soc. 2009, 131, 8108–8120; b) V. A. Livshits, B. G. Dzikovski, D. Marsh, J. Magn. Reson. 2001, 148, 221–237.
- [30] a) S. W. Chang, A. R. Lewis, K. E. Prosser, J. R. Thompson, M. Gladkikh, M. B. Bally, J. J. Warren, C. J. Walsby, *Inorg. Chem.* 2016, 55, 4850–4863;
 b) A. R. Timerbaev, C. G. Hartinger, S. S. Aleksenko, B. K. Keppler, *Chem. Rev.* 2006, 106, 2224–2248;
 c) T. C. Johnstone, K. Suntharalingam, S. J. Lippard, *Chem. Rev.* 2016, 116, 3436–3486.
- [31] Y. Gou, J. Qi, J.-P. Ajayi, Y. Zhang, Z. Zhou, X. Wu, F. Yang, H. Liang, Mol. Pharmaceutics 2015, 12, 3597–3609.
- [32] J. R. Pilbrow, Transition Ion Electron Paramagnetic Resonance, Clarendon, Oxford, 1990.
- [33] a) J. A. Weil, J. R. Bolton, Electron Paramagnetic Resonance: Elementary Theory and Practical Applications, Wiley, Hoboken, 2007; b) N. N. Murthy, K. D. Karlin, I. Bertini, C. Luchinat, J. Am. Chem. Soc. 1997, 119, 2156– 2162; c) I. Bertini, C. Luchinat, G. Parigi, E. Ravera, Solution NMR of Paramagnetic Molecules: Applications to Metallobiomolecules and Models, Elsevier, Amsterdam, 2015; d) K. E. Prosser, A. W. Y. Leung, S. Harrypersad, A. R. Lewis, M. B. Bally, C. J. Walsby, Chem. Eur. J. 2018, 24, 6334– 6338.
- [34] C. Hansch, A. Leo, R. W. Taft, Chem. Rev. 1991, 91, 165-195.
- [35] A. J. Bard, L. R. Faulkner, *Electrochemical Methods: Fundamentals and Applications*, 2nd ed., Wiley, New York, **2001**.
- [36] a) F. Q. Schafer, G. R. Buettner, Free Radical Biol. Med. 2001, 30, 1191–1212; b) J. Hancock, M. Whiteman, ROS 2018, 5, 78–85; c) L. E. Jamieson, A. Jaworska, J. Jiang, M. Baranska, D. J. Harrison, C. J. Campbell, Analyst 2015, 140, 2330–2335.
- [37] J. Jiang, C. Auchinvole, K. Fisher, C. J. Campbell, Nanoscale 2014, 6, 12104–12110.
- [38] G. G. Martinovich, S. N. Cherenkevich, H. Sauer, Eur. Biophys. J. 2005, 34, 937–942.
- [39] S. G. Mayhew, Eur. J. Biochem. 1978, 85, 535-547.
- [40] D. T. Richens, Chem. Rev. 2005, 105, 1961-2002.
- [41] A. Haase, J. Frahm, D. Matthaei, W. Hanicke, K. D. Merboldt, J. Magn. Reson. 1986, 67, 258–266.
- [42] a) J. Hennig, A. Nauerth, H. Friedburg, Magn. Reson. Med. 1986, 3, 823–833; b) A. Mastropietro, E. Bernardi, L. Breschi Gian, I. Zucca, M. Cametti, D. Soffientini Chiara, M. Curtis, G. Terraneo, P. Metrangolo, R. Spreafico, G. Resnati, G. Baselli, Magn. Reson. Imaging 2013, 40, 162–170.
- [43] B. S. Cummings, R. G. Schnellmann, Curr. Protoc. Pharmacol. 2004, 25, 12.18.11-12.18.22.
- [44] L. C. Crowley, B. J. Marfell, N. J. Waterhouse, *Cold Spring Harb. Protoc.* **2016**, *2016*, DOI: 10.1101/pdb.prot087205.
- [45] U. Ziegler, P. Groscurth, *Physiology* **2004**, *19*, 124–128.
- [46] S. P. Oldfield, M. D. Hall, J. A. Platts, J. Med. Chem. 2007, 50, 5227–5237.



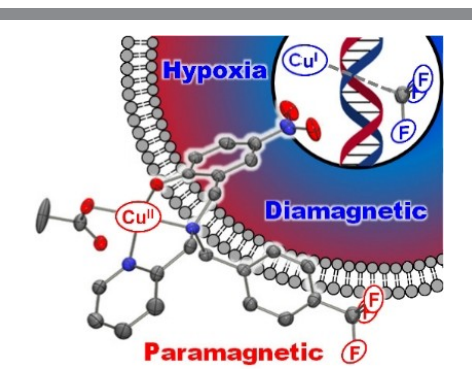
- [47] Test No. 107: Partition Coefficient (n-octanol/water): Shake Flask Methods, OECD Publishing, 1995.
- [48] C. A. Puckett, R. J. Ernst, J. K. Barton, Dalton Trans. 2010, 39, 1159-1170.
- [49] C. A. Puckett, J. K. Barton, Biochemistry 2008, 47, 11711–11716.
- [50] J. H. Kaplan, B. Maryon, Biophys. J. 2016, 110, 7-13.
- [51] K. Suzuki, P. Bose, R. Y. Leong-Quong, D. J. Fujita, K. Riabowol, BMC Res. Notes 2010, 3, 294.
- [52] a) E. Lamour, S. Routier, J.-L. Bernier, J.-P. Catteau, C. Bailly, H. Vezin, J. Am. Chem. Soc. 1999, 121, 1862–1869; b) B. K. Santra, P. A. N. Reddy, G. Neelakanta, S. Mahadevan, M. Nethaji, A. R. Chakravarty, J. Inorg. Biochem. 2002, 89, 191–196; c) J. Liu, T. Zhang, T. Lu, L. Qu, H. Zhou, Q. Zhang, L. Ji, J. Inorg. Biochem. 2002, 91, 269–276.
- [53] S. Antony, J. B. Aitken, S. Vogt, B. Lai, T. Brown, L. Spiccia, H. H. Harris, J. Biol. Inorg. Chem. 2013, 18, 845–853.
- [54] a) M. Klajner, C. Licona, L. Fetzer, P. Hebraud, G. Mellitzer, M. Pfeffer, S. Harlepp, C. Gaiddon, *Inorg. Chem.* 2014, 53, 5150–5158; b) S. W. Botchway, M. Charnley, J. W. Haycock, A. W. Parker, D. L. Rochester, J. A. Weinstein, J. A. G. Williams, *Proc. Natl. Acad. Sci. USA* 2008, 105, 16071–16076.
- [55] E. J. Lanni, S. S. Rubakhin, J. V. Sweedler, J. Proteomics 2012, 75, 5036–5051.
- [56] S. Routier, J.-L. Bernier, M. J. Waring, P. Colson, C. Houssier, C. Bailly, J. Org. Chem. 1996, 61, 2326–2331.
- [57] E. J. Billo, Inorg. Nucl. Chem. Lett. 1974, 10, 613–617.
- [58] a) A. R. Chakravarty, P. A. N. Anreddy, B. K. Santra, A. M. Thomas, J. Chem. Sci. 2002, 114, 391–401; b) J. William Lown, S.-K. Sim, Biochem.

- Biophys. Res. Commun. 1977, 77, 1150–1157; c) V. Rajendiran, R. Karthik, M. Palaniandavar, V. S. Periasamy, M. A. Akbarsha, B. S. Srinag, H. Krishnamurthy, Inorg. Chem. 2007, 46, 8208–8221.
- [59] a) R. Anjum, D. Palanimuthu, D. S. Kalinowski, W. Lewis, K. C. Park, Z. Kovacevic, I. U. Khan, D. R. Richardson, *Inorg. Chem.* 2019, 58, 13709–13723; b) M. H. Torre, D. Gambino, J. Araujo, H. Cerecetto, M. Gonzalez, M. L. Lavaggi, A. Azqueta, A. Lopez de Cerain, A. M. Vega, U. Abram, A. J. Costa-Filho, *Eur. J. Med. Chem.* 2005, 40, 473–480; c) C. Urquiola, D. Gambino, M. Cabrera, M. L. Lavaggi, H. Cerecetto, M. Gonzalez, A. Lopez de Cerain, A. Monge, A. J. Costa-Filho, M. H. Torre, *J. Inorg. Biochem.* 2008, 102, 119–126.
- [60] C. Urquiola, D. Gambino, M. Cabrera, M. L. Lavaggi, H. Cerecetto, M. González, A. L. de Cerain, A. Monge, A. J. Costa-Filho, M. H. Torre, J. Inorg. Biochem. 2008, 102, 119–126.
- [61] Y. Hatori, S. Clasen, N. M. Hasan, A. N. Barry, S. Lutsenko, J. Biol. Chem. 2012, 287, 26678–26687.
- [62] K. Katano, A. Kondo, R. Safaei, A. Holzer, G. Samimi, M. Mishima, Y.-M. Kuo, M. Rochdi, S. B. Howell, Cancer Res. 2002, 62, 6559–6565.

Manuscript received: February 16, 2021 Accepted manuscript online: April 20, 2021 Version of record online:

FULL PAPER

Fluorine-labelled Cu^{II} complexes have been developed as hypoxiatargeting chemotherapeutics and MRI agents. Tuning the electronic properties identified a nitro-substituted complex as having hypoxia-selective cytotoxicity driven by nuclear accumulation and DNA cleavage. ¹⁹F magnetic resonance experiments discriminate between Cu^{II} and reduced complexes, thus demonstrating a bifunctional role for Cu^{II} complexes as both hypoxia probes and chemotherapeutic agents.



Dr. K. E. Prosser, Dr. D. Xie, A. Chu, G. A. MacNeil, B. R. Varju, R. T. Kadakia, Prof. E. L. Que*, Prof. C. J. Walsby*

1 – 12

Copper(II) Pyridyl Aminophenolates: Hypoxia-Selective, Nucleus-Targeting Cytotoxins, and Magnetic Resonance Probes

